

Cite this: DOI: 00.0000/xxxxxxxxxx

Supplementary Information: Stable antiferromagnetic nanocrystals for room temperature applications: the case of iron nitride

Iwona Agnieszka Kowalik,^a Nevill Gonzalez Szwacki,^b Miguel Ángel Niño,^c Francisco Jesús Luque,^d and Dimitri Arvanitis,^{*e}

Received Date

Accepted Date

DOI: 00.0000/xxxxxxxxxx

1 Sample growth

We investigate (Ga,Fe)N, δ -(Ga,Fe)N and Fe_nN/GaN films grown at the Kepler University Linz-Austria by metal organic vapour phase epitaxy (MOVPE) on c-axis oriented sapphire substrates.^{1,2} The films investigated here have been selected from a series of samples, whose composition and structural properties were examined by secondary-ion mass spectroscopy, synchrotron x-ray diffraction, transmission electron microscopy, dispersive x-ray spectroscopy, extended x-ray absorption fine-structure and x-ray absorption near-edge structure.^{1,2} In this communication we extend the results of earlier studies by investigating the surface and the near surface region of selected samples with a probing depth of about up to 5 nm.

The size and composition of the Fe_nN nanocrystals we study is steered by means of the sample growth parameters and procedure.³ The type of sample morphology we present is indicated in Fig. 1(a)-(c). In the growth the precursors trimethylgallium (TMGa), ammonia (NH₃), and ferrocene (Cp₂Fe) were used. Using a growth procedure called substrate nitridation² at high growth temperature of the substrate, T_g, of 900°C, for

(Ga,Fe)N samples Nr 987 and 988 (Fig. 1(a)) we obtain smaller Fe-rich magnetic nanocrystals embedded in the GaN matrix² with typical sizes as observed by PEEM in the near surface region between 50 to 100 nm.⁴ The flow rate of the Fe precursor was set at 100 and 300 standard cubic centimeters per minute (sccm) respectively for samples Nr 987 and 988. By changing the growth procedure to δ -growth on the Ga precursor,⁵ planar arrays of Fe rich nanocrystals can be formed (δ -(Ga,Fe)N samples 1650 and 1651, Fig. 1(b)). For the growth of these layers the flow was set at 800 sccm for the NH₃ source, 5 sccm for the TMGa source and 450 sccm for the Cp₂Fe source. For samples 1650 and 1651 were grown 30 and 15 δ -periods, respectively, at a substrate temperature of 780°C. For this type of δ -grown samples, the nanocrystals were deposited directly on the GaN surface, in contrast to previous samples where the nanocrystals were capped with a GaN layer.² It is finally possible, using controlled sample annealing, to directly obtain Fe_nN nanocrystals on the GaN surface by means of fragmenting a thin Fe_nN film deposited on the GaN surface (samples 1303 and 1311, Fig. 1(c)). Here the temperature of the substrate, T_g, was set at 750°C. For these two samples the partial pressure of the NH₃/H₂ gases used during the growth in the reactor, was different.

Prior to the XPEEM and XMCD-PEEM characterisation, each sample was characterised *in situ* by means of Low Energy Electron Microscopy (LEEM).⁶ LEEM is a very surface sensitive technique and characterises therefore the surface morphology (Fig. S1 (a) and (b)). The surfaces of the films represented by sample 1311 are composed of nanoparticles with flat tops with a clear bright contrast in LEEM with respect to the matrix, indicating their good crystalline order. The major number of particles have diameter between 25 and 50 nm (figures close to the microscope resolution) with a circular shape (Fig. S1 (d)). A small number of larger nanoparticles also exist with a diameter of around 100 nm, the largest we found being about 500 nm in diameter, becoming

^a Institute of Physics, Polish Academy of Sciences, al. Lotników 32/46, 02-668 Warsaw, Poland

^b Institute of Theoretical Physics, Faculty of Physics, University of Warsaw, 00-681 Warsaw, Poland

^c IMDEA Nanociencia, Campus de Cantoblanco E-28049 Madrid, Spain

^d Depto. de Física de la Materia Condensada, Universidad Autónoma de Madrid, E-28049, Madrid, Spain

^e Department of Physics and Astronomy, Uppsala University, P.O. Box 516, 751 20 Uppsala, Sweden. E-mail: dimitri.arvanitis@physics.uu.se

† Electronic Supplementary Information (ESI) available: [details of any supplementary information available should be included here]. See DOI: 00.0000/00000000.

‡ Additional footnotes to the title and authors can be included e.g. 'Present address:' or 'These authors contributed equally to this work' as above using the symbols: ‡, §, and ¶. Please place the appropriate symbol next to the author's name and include a

\footnotetext entry in the the correct place in the list.

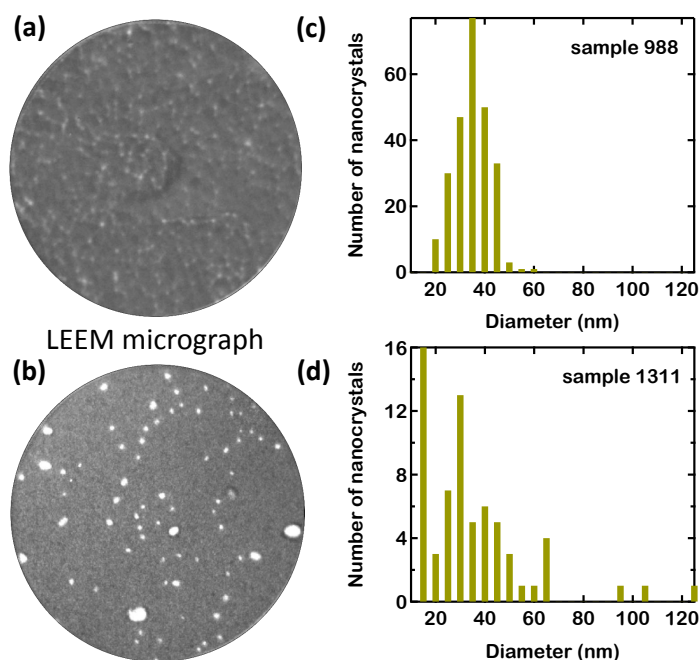


Fig. S 1 LEEM micrographs measured for samples 988 (a) and 1311 (b) with field of view of $2 \mu\text{m}$. Histogram of the size distribution of the nanocrystals for sample 988 (c) and 1311 (d).

slightly elongated. The nanoparticles have a random distribution over the surface with no specific order, and their density is about 22 nanoparticles per μm^2 . For the larger nanoparticles it is possible to obtain a quantitative chemical composition determination of a single particle, using the Fe L-edges and N K-edge x-ray absorption spectra from the XPEEM images (Fig. S2). This results in a uniform distribution of the Fe and N atoms within the nanocrystals.

For samples of the family represented by sample 988 the LEEM images show the existence of slightly smaller circular nanoinclusions versus the sample family 1311 nanoparticles, with a more narrow distribution of typical sizes centered at 35 nm and with a circular shape (Fig. S1 (c)). The surface shows terraces of hexagonal shape, probably related to the sapphire substrate crystallography, with quite straight edges with the nanoinclusions distributed more uniformly over the terraces of the surface. The LEEM contrast (as well as the magnetic contrast which is possible to observe in Fig. S3) is much weaker as compared with the other sample type. The particle edges are less definite, sometimes exhibiting a halo, features compatible with a location of the nanocrystals just below the surface. The density of nanoinclusions is more than three times higher versus the other type of sample, 80 nanoinclusions per μm^2 . A quantitative XPEEM chemical composition analysis for this family has been presented earlier.⁴

The magnetic properties were characterised for some of these types of samples (sample (a) from Fig. 1) using superconducting quantum interference device (SQUID) magnetometry.^{2,7} Following the temperature and magnetic field dependence of the magnetisation for these samples both a ferromagnetic (FM) and paramagnetic response has been associated with the presence of Fe

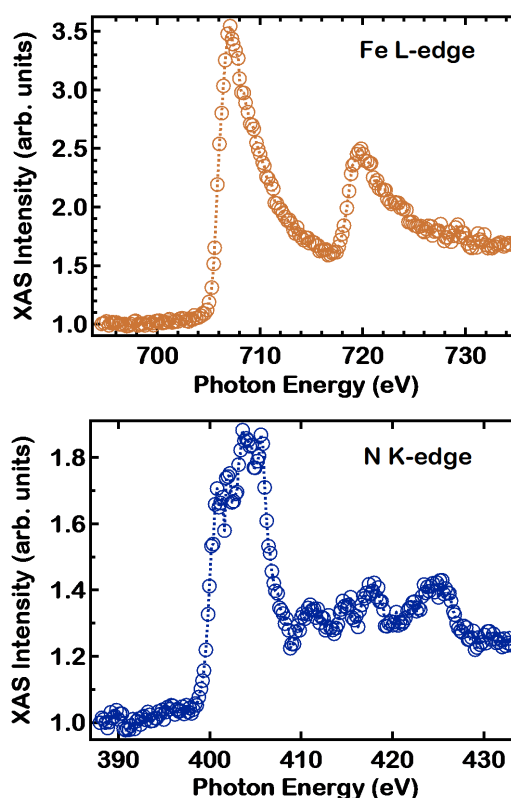


Fig. S 2 XAS measured for a single representative nanocrystal of the sample 1311 at the N-Kedge and the Fe-L edges.

atoms in the (Ga,Fe)N films. The ferromagnetic response has been assigned to the existence of the Fe_nN nanocrystals within the GaN matrix.^{2,4} The paramagnetic response at low temperatures has been linked with the existence of substitutional Fe atoms in the GaN matrix.² For results at room temperature we discuss here, another possibility is the existence of small size nanocrystals in the paramagnetic state. Interestingly, these samples show also a magnetisation component which is linear versus magnetic field and is barely dependent on temperature.² Such a field dependence is typical of an antiferromagnetic (AFM) component of the magnetization, which could be explained by the existence of antiferromagnetic nanocrystals.

The SQUID results indicate indeed, that the total Fe ion concentration contributing to the paramagnetic and ferromagnetic signals is smaller versus the one resulting from the SIMS data.² The existence of antiferromagnetic nanocrystals would explain this observation. However, using only the SQUID data, direct experimental evidence for the existence of antiferromagnetic nanocrystals and the value of their magnetic moment is not easy to obtain. SQUID magnetometry probes the magnetic response, not only of the surface but also of the bulk of the samples. In this communication we focus on measurements of the surface and near surface region of the films, using photon-in, electron-out core level spectroscopy tools. One cannot therefore directly compare the SQUID results with the results obtained by means of XMCD and XLMD spectroscopy.

2 XPEEM and XMCD-PEEM

Our studies employing X-ray Photo Emission Electron Microscopy (XPEEM), both in the X-ray Absorption Spectroscopy (XAS) and X-ray Magnetic Circular Dichroism (XMCD) modes, have been performed at the Nanospectroscopy beam line at the Elettra Synchrotron facility in Trieste-Italy with a lateral resolution down to 40 nm.^{8,9} A grazing x-ray incidence angle of 16° versus the sample surface plane is used.⁸ The data are taken at room temperature. For the XPEEM data in the XAS mode linearly polarized x-rays are used and for the XMCD-PEEM data circularly polarized x-rays. The photon energy for the XPEEM micrographs for panels (d) and (e) is set to the maximum of the Fe L_3 and L_2 white lines. The XPEEM measurements were performed in the virgin magnetic state, no external magnetic field was applied. In Fig. 1 XPEEM micrographs are shown in the direct XAS mode, which characterise the chemical state of the near surface region. In the XAS mode, XPEEM allows for chemical mapping of the near surface region by collecting secondary electrons emitted after photon absorption. When the incident photon energy corresponds to the absorption edge of an element on the surface or residing down to several nanometers below, a significant increase is observed in the secondary electron emission from the areas where the specific element appears. Here we have focused on the L_3 and L_2 white line photon energies, in order to increase the reliability of the spatially resolved XAS and the sensitivity to the regions of the samples with the least Fe concentration.

The smaller nanocrystals identified by XPEEM in Fig. 1 (e) are of order 100 nm in lateral size, the larger ones of order 500 nm. For the $\text{Fe}_x\text{N}/\text{GaN}$ sample 1311 (Fig. 1 (e)) the regions of the sample without nanocrystals do exhibit a much darker contrast indicative of the fact that in this case much less substitutional Fe is present in the GaN matrix versus the sample where the Fe_xN nanocrystals are embedded in the GaN lattice (Fig. 1 (d)). This is particularly clear for the case of Fig. 1 (e), where for some regions of the sample also a spectral analysis was performed.¹⁰ The Fe_xN nanocrystal size and Fe content within the GaN matrix discussed here is in agreement with earlier results for this set of samples.⁴

In Fig. 1 and Fig. S3 also XPEEM difference micrographs in the XMCD mode are shown, to characterise the magnetic state of the samples. To obtain difference micrographs in the XMCD mode, two XPEEM micrographs are recorded using x-rays of opposite helicity, by keeping all other parameters of the experiment fixed. The micrograph intensities obtained are then subtracted pixel by pixel. In the corresponding XMCD difference micrograph only the topographic features exhibiting magnetic contrast are visible. Here we use measurements at both the Fe L_3 and L_2 white line photon energies (Fig. S3). For the XMCD-PEEM data, difference micrographs are shown to characterize the magnetic state of the sample. Here given that micrographs are subtracted with the same topographic features, only the parts of the sample with the magnetisation along the propagation direction of the x-ray beam are indeed visible. Clear dichroic contrast is seen for several of the nanocrystals in Fig. 1 (d) for the XMCD-PEEM micrographs. The contrast is indeed of magnetic origin, as it is inverted using photon energies at the L_3 and L_2 edge maxima (Fig. S3). Not all

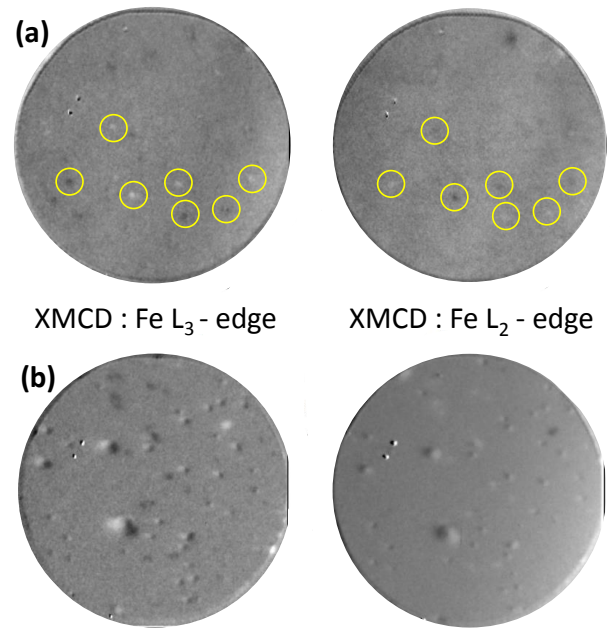


Fig. S 3 XMCD-PEEM micrographs measured at both the Fe L_3 and L_2 white line photon energies for (a) sample 988 and (b) sample 1311 with a field of view of $2\ \mu\text{m}$, showing the same region. The magnetic contrast of the Fe atoms in the ferromagnetic state is known to revert between the Fe L_3 and L_2 white line photon energies.

nanocrystals which are resolved in the XMCD micrographs (Fig. 1 (d,e)) do exhibit ferromagnetic contrast. For sample 988 about 50% of the nanocrystals appear to be ferromagnetically live. This is seen also for sample 1311 in the case of the smaller nanocrystals.

Given the fact that we use a grazing x-ray incidence angle of 16° versus the sample surface plane⁸, we are mostly sensitive to the magnetization component within the surface plane along the direction of the incident x-rays. We cannot, using only the XMCD-PEEM micrographs, characterise a different magnetization direction for the nanocrystals which do not exhibit a magnetic contrast here. In the case of sample 1311 we observe that the percentage of ferromagnetic nanocrystals is higher. This sample contains also larger Fe_xN nanocrystals which are ferromagnetic according to the XMCD-PEEM data of Fig. 1 (e). Indeed a clear magnetic domain structure can be seen in the case of the larger nanocrystals for sample 1311. The type of magnetic contrast recorded indicates a spin arrangement within these nanocrystals of the vortex type.^{10,11}

3 X-ray absorption measurements

XAS, XMCD and X-ray Linear Magnetic Dichroism (XLMD) measurements, without making use of microscopy, but using applied magnetic fields up to 0.6 T, have been carried out at the beam line I1011 of the MAX-lab synchrotron radiation laboratory, Sweden.¹² At the I1011 beamline, the Elliptically Polarizing Undulator x-ray source allows to take XAS spectra with soft x-rays of a polarisation state both close to circular or linear. Linear x-rays can be produced with the plane of polarisation either in the storage

ring plane or perpendicular to it. The measurements are performed in the Total Electron Yield (TEY) mode by measuring the photocurrent of the sample. In the TEY mode the effective mean free path of the electrons is of the order of 2 nm, implying that only a region of order 5 nm below the sample surface is probed in this mode. Linear (with a degree of linear polarization of 0.95) or close to circular x-ray polarization (with a degree of circular polarization of 0.85) are used in XAS, XLMD and XMCD investigations. XAS measurements were performed as a function of the angle of x-ray incidence. At beam line I1011 the samples were introduced into a Ultra High Vacuum chamber, equipped with eight coils allowing for a magnetic field of 0.5T to be applied in any space direction.¹⁰ At beam line I1011 the x-ray linear magnetic dichroism (XLMD) measurements were retrieved orienting the applied magnetic field parallel or perpendicular to the polarisation plane of the x-rays. Linear x-rays are used in this case. The electric field is applied in both cases along equivalent crystallographic directions of the GaN lattice to avoid any intensity variations in the XAS spectra of non magnetic origin. A magnetic field of $H = \pm 0.5$ T serves to fix the magnetisation direction for the XLMD experiments.

XAS and XMCD measurements under applied external magnetic field up to 6T were performed on selected samples at the BOREAS beam line of ALBA, Spain (Fig. 2 (a)). The x-ray absorption spectra at BOREAS are taken using the sample photocurrent in the TEY mode. A magnetic field of $H = \pm 6$ T serves to reverse the magnetisation direction for the evaluation of the x-ray magnetic circular dichroism (XMCD) magnitude at 300 K. Given the higher energy of the storage ring a higher photon flux is available allowing for a higher photon energy resolving power versus the data of Fig. 2 (b) taken at the I1011 beam line of MAX IV-lab. Sample 1311 is investigated at both beam lines.

The samples as introduced into the ultra high vacuum end stations for the XAS measurements show x-ray absorption specific to C and O atom impurities, which disappears after *in situ* soft sputtering with Ar^+ ions. We have used the Ar^+ energy of 1 keV over the sputtering cycle of 10 min. Typically two sputter cycles have been used. To leave Fe-rich nanocrystals unaffected, no annealing has been carried out. The soft x-ray range between 0.2 and 1.5 keV was used to characterise the chemical composition of the samples. No sizeable contamination was detected in this energy range, only the expected N K-edge and L-edges of Fe and Ga were detected in this energy range.⁴

The spatially integrated XMCD results indicate that even in the presence of high applied magnetic fields the XMCD response per Fe atom does not approach the expected values. It is relevant to point out that for the samples from the (Ga,Fe)N family, such as sample 987, only about half of the larger nanocrystals do exhibit ferromagnetic contrast in Fig. 1(d). In combination with the XPEEM and XMCD-PEEM micrographs, as observed in Fig. 1 where only roughly half the larger nanocrystals exhibit ferromagnetic contrast, the possibility arises that even for larger nanocrystals no ferromagnetic response is recorded. Turning to the data of Fig. 2 (b) we note that a substantial magnetic response is recorded for this sample also in the XLMD mode. The absence of an XMCD magnetic response of sufficient magnitude as ob-

served in Fig. 2 (a) at high magnetic fields, and the presence of a sizeable XLMD signal (Fig. 2 (b)) is an indication for the existence of magnetic moments also in an antiparallel arrangement. In this context it is relevant to also discuss the XPEEM and XMCD-PEEM micrographs of Fig. 1 (d). In the case of sample 988 it is indeed observed that nanocrystals which are clearly identified in the XPEEM mode, do not exhibit ferromagnetic contrast in the XMCD-PEEM mode. This lack of ferromagnetic response, can also be caused by the existence of nanocrystals in an antiferromagnetic state, and not only by the specific geometry chosen in this particular experiment and by the lack of lateral resolution.

4 First-principles and multiple scattering calculations

Our first-principles calculations are based on DFT and are performed using a plane-wave basis and Troullier-Martins norm-conserving pseudo-potentials as implemented in the Quantum-ESPRESSO package.¹³ For the exchange and correlation functional, we employ the hybrid HSE06 exchange-correlation functional. The plane-wave basis with a 60 Ry energy cutoff is sufficient to achieve energy convergence. A $8 \times 8 \times 8$ k -point mesh is used for the Brillouin-zone integrations. A Gaussian smearing of 0.014 eV is used for the initial occupations. Bulk Fe_4N has a cubic perovskite-type structure (space group $Pm\bar{3}m$) with a lattice constant of 3.795 Å. Our calculations give a lattice constant of 3.779 Å, in fair agreement with the experimental value. We have also obtained a similar agreement between computed and experimental values for the rest of the studied Fe_nN phases. The calculations are done using supercells corresponding to conventional unit cells. Since HSE06 calculations are computationally very demanding in comparison to PBE ones, the structural optimisation of cell parameters and atomic positions is carried out at the PBE level of theory, and the final relaxed structures are taken for the HSE06 calculations. The HSE06 exchange and correlation functional, that we use in our calculations, is substantially better than the popular PBE functional. It can however, still be improved by tuning its default parameters.¹⁴ This can be important for the description of the electronic properties of certain materials or inorganic systems.¹⁵ The use of the HSE06 functional does not constitute a limiting factor within the level of accuracy needed here. A detailed discussion of the limitations introduced by the use of the HSE06 functional goes beyond the scope of the present communication.

The FEFF code is an *ab initio*, self-consistent, multiple scattering code for the simultaneous calculations of excitation spectra and electronic structure.¹⁶ Here we work with the real space option of the FEFF9 code. We have presented FEFF results of the XAS and XMCD Fe_nN phases previously, using real space structures as obtained from literature.⁴ Here we use the calculated real space structures obtained by the structural optimisation by means of DFT as described above, leading to the calculated magnetic moments as shown in Fig. 3 (b) and (c).

Notes and references

- 1 A. Bonanni, M. Kiecana, C. Simbrunner, T. Li, M. Sawicki, M. Wegscheider, M. Quast, H. Przybylinska, A. Navarro-Quezada, R. Jakiela, A. Wolos, W. Jantsch and T. Dietl, *Phys. Rev. B*, 2007, **75**, 125210.
- 2 A. Navarro-Quezada, W. Stefanowicz, T. Li, B. Faina, M. Rovezzi, R. T. Lechner, T. Devillers, G. Bauer, M. Sawicki, T. Dietl and A. Bonanni, *Phys. Rev. B*, 2010, **81**, 205206.
- 3 A. Bonanni and T. Dietl, *Chem. Soc. Rev.*, 2010, **39**, 528.
- 4 I. A. Kowalik, A. Persson, M. Á. Niño, A. Navarro-Quezada, B. Faina, A. Bonanni, T. Dietl and D. Arvanitis, *Phys. Rev. B*, 2012, **85**, 184411.
- 5 A. Navarro-Quezada, T. Devillers, T. Li and A. Bonanni, *App. Phys. Lett.*, 2012, **101**, 081911.
- 6 E. Bauer, *Rep. Prog. Phys.*, 1994, **57**, 895.
- 7 T. Dietl, K. Sato, T. Fukushima, A. Bonanni, M. Jamet, A. Barski, S. Kuroda, M. Tanaka, P. N. Hai and H. Katayama-Yoshida, *Rev. Mod. Phys.*, 2015, **87**, 1311.
- 8 A. Locatelli and E. Bauer, *J. Phys.: Condens. Matter*, 2008, **20**, 093002.
- 9 T. O. Menteş, G. Zamborlini, A. Sala and A. Locatelli, *Beilstein J. Nanotechnol.*, 2014, **5**, 1873.
- 10 I. A. Kowalik, *Acta Phys. Pol. A*, 2015, **127**, 831.
- 11 S. D. Col, S. Jamet, N. Rougemaille, A. Locatelli, T. O. Mentes, B. S. Burgos, R. Afid, M. Darques, L. Cagnon, J. C. Toussaint and O. Fruchart, *Phys. Rev. B*, 2014, **89**, 180405(R).
- 12 I. A. Kowalik, G. Öhrwall, B. N. Jensen, R. Sankari, E. Wallén, U. Johansson, O. Karis and D. Arvanitis, *J. Phys. Conf. Series*, 2010, **211**, 012030.
- 13 P. Giannozzi, S. Baroni, N. Bonini, M. Calandra, R. Car, C. Cavazzoni, D. Ceresoli, G. L. Chiarotti, M. Cococcioni, I. Dabo, A. Dal Corso, S. de Gironcoli, S. Fabris, G. Fratesi, R. Gebauer, U. Gerstmann, C. Gougoussis, A. Kokalj, M. Lazzeri, L. Martin-Samos, N. Marzari, F. Mauri, R. Mazzarello, S. Paolini, A. Pasquarello, L. Paulatto, C. Sbraccia, S. Scandolo, G. Sclauzero, A. P. Seitsonen, A. Smogunov, P. Umari and R. M. Wentzcovitch, *J. Phys. Condens. Matter*, 2009, **21**, 395502.
- 14 J. E. Moussa, P. A. Schultz¹ and J. R. Chelikowsky, *J. Chem. Phys.*, 2012, **136**, 204117.
- 15 M. E. Foster, J. D. Azoulay, B. M. Wong and M. D. Allendorf, *Chem. Sci.*, 2014, **5**, 2081.
- 16 J. J. Rehr and R. C. Albers, *Rev. Mod. Phys.*, 2000, **72**, 621.